THE JOURNAL OF PHYSICAL CHEMISTRY B

Article

pubs.acs.org/JPCB

Order, Viscoelastic, and Dielectric Properties of Symmetric and Asymmetric Alkyl[1]benzothieno[3,2-b][1]benzothiophenes

Christos Grigoriadis,[†] Claude Niebel,[‡] Christian Ruzié,[‡] Yves H. Geerts,[‡] and George Floudas*[,†,§]

[†]Department of Physics, University of Ioannina, 45110 Ioannina, Greece

[‡]Laboratoire de Chimie des Polymères CP 206/01, Faculté des Sciences, Université Libre de Bruxelles (ULB), 1050 Brussels, Belgium

[§]Max-Planck Institute for Polymer Research, Mainz, Germany

Supporting Information

ABSTRACT: The morphology, the viscoelastic, the dielectric properties and the dynamics of phase transformation are studied in symmetrically and asymmetrically substituted alkyl[1]benzothieno[3,2-*b*][1]benzothiophenes (C_8-BTBT) by X-ray scattering, rheology, and dielectric spectroscopy. The interlayer spacing reflects the molecular and supramolecular ordering, respectively, in the symmetrically and asymmetrically substituted BTBTs. In the asymmetric BTBT, the core layer is double in size with a broader network of intermolecular interactions though the increased S−S contacts that is prerequisite for the development of high performance OFET devices. Two crystal states with elastic and viscoelastic responses were identified in the symmetric compound. In contrast, the SmA phase in the asymmetric compound is a viscoelastic solid. A path-dependent dielectric environment with a switchable dielectric permittivity was found in both compounds by cooling below 0 °C with possible implications to charge transport. The kinetics of phase transformation to the crystalline and SmA phases revealed a nucleation and growth mechanism with rates dominated by the low activation barriers.

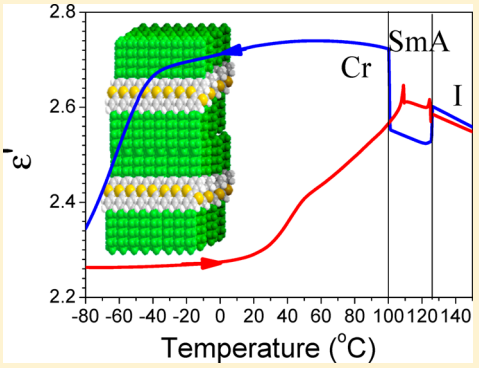

I. INTRODUCTION

The emergence of flexible and printed electronics is likely to produce a new technological evolution in field-effect transistors. In particular, organic field-effect transistors (OFETs) have been designed and developed over the past two decades.[1] An attractive feature of organic semiconductor materials is their solubility and the possibility of preparing thin films of high crystallinity by simple fabrication processes such as spin-coating, drop-casting, or more elaborate methods such antisolvent crystallization[2] or fluid-enhanced crystal engineering.[3,4] Some of the highest charge carrier mobilities for thin film OFETs have been reported for 2,7-dialkyl[1]benzothieno[3,2-*b*][1]benzothiophene (C_n-BTBT-C_n). The synthesis of mainly symmetric BTBTs[5−10] as well as the promising device characteristics (with a maximum charge carrier mobility value of 31 $m^2/(V\,s)$ and an average value of about 17 $m^2/(V\,s)$) was recently reported.[8,1] In these systems, a lamellar structure composed of alternating alkyl layers and BTBT layers, the latter with a herringbone structure, facilitates an efficient two-dimensional (2D) charge carrier transport. Charge transport in 2D is advantageous when compared to 1D systems, as discotic liquid crystals, where charge mobility along the columnar axis is limited by defects.[11−13] Progress in this field requires a methodology that best combines material design with processing and fabrication techniques. Issues related to long-term stability, device reliability and reproducibility, morphology, electrical characteristics, and processability need to be addressed in detail if these promising materials are realized for market applications.

In the present work, we report on the thermodynamic, structural, viscoelastic, and dielectric properties of two molecules, namely 2,7-dioctyl[1]benzothieno[3,2-*b*][1]-benzothiophene (C_8-BTBT-C_8) and the corresponding asymmetric compound (C_8-BTBT). Although these molecules belong to the class of most efficient OFETs, their thermodynamic, viscoelastic, and dielectric properties have not been investigated. It is essential to clarify how side-chain substitution affects the thermodynamic/structural properties. In addition, knowledge of the viscoelastic properties of phases is of importance when it comes to devices and device fabrication. The dielectric permittivity within each phase is needed especially when the charge carrier mobility is extracted from the characteristic electrical measurements. In the last part, we explore the kinetics of phase transformation that define the limits of thermodynamic stability (spinodals) of the different phases. The results presented here could be employed as guidelines during device fabrication especially when crossing the phase boundaries. Moreover, the information gathered on the dynamics of BTBT compounds, currently among the best performing organic semiconductors, will be of interest to device physics because the interplay between molecular packing,

Received: December 19, 2013
Revised: January 17, 2014
Published: January 17, 2014

   dx.doi.org/10.1021/jp412422e | *J. Phys. Chem. B* 2014, 118, 1443−1451

polarizability and charge transport is the subject of intense research and debate.[14] In particular, the temperature dependence of charge carrier mobility currently cannot be explained.[15]

II. EXPERIMENTAL SECTION

Synthesis. C_8-BTBT and C_8-BTBT-C_8 have been synthesized from BTBT following literature procedures (Figure S1, Supporting Information).[16−18] Their structural identity has been assessed by ^{1}H NMR spectroscopy. Purification has been carried out by column chromatography and recrystallization. ^{1}H NMR spectroscopy and thin layer chromatography have been used to assess purity according to classical procedures.[9] Electrically active traces of impurities are discussed in Supporting Information. However, no impurities have been detected by these techniques (Figure S2, Supporting Information).

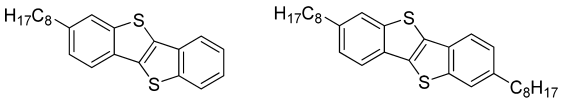

C_8-BTBT C_8-BTBT-C_8

Differential Scanning Calorimetry (DSC). The thermal behavior of the compounds was studied by differential scanning calorimetry on cooling and subsequent heating at a rate of 10 K/min with a Mettler 30 DSC. The DSC traces from the second cooling and heating scans are shown in Figure 1. The figure shows some strong phase transitions (of first order) and a much broader phase transformation (it is actually a double peak) in C_8-BTBT at lower temperatures. The transition temperatures and associated heats of fusion on cooling and heating are summarized in Table 1.

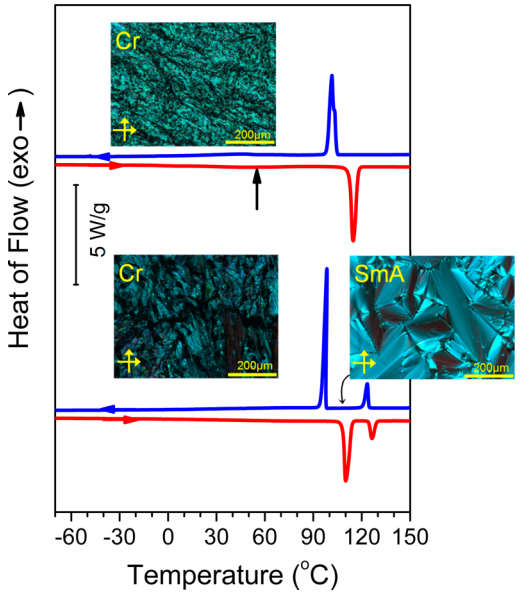

Figure 1. DSC traces of C_8-BTBT (top) and C_8-BTBT-C_8 (bottom) obtained during cooling (blue) and subsequent heating (red) with 10 K/min. Arrows indicate the direction of temperature change. The vertical arrow in C_8-BTBT, signify a broad transition between two crystalline phases. POM images are also shown corresponding to the Cr phase at T = 100 °C for C_8-BTBT and to the Cr and SmA phases of C_8-BTBT-C_8 at T = 95 °C and T = 110 °C, respectively.

Table 1. Transition Temperatures and Associated Heats Obtained on Heating (DSC rate 10 K/min)

compound	transition	temperature [°C]	ΔH [J g^{-1}]
C_8-BTBT	$Cr_B \rightarrow Cr_A$	~55.0	19.0
	$Cr_A \rightarrow I$	114.8	82.6
C_8-BTBT-C_8	Cr→SmA	110.1	67.8
	SmA→I	126.4	16.1

Polarizing Optical Microscopy (POM). A Zeiss Axioskop 40, equipped with a video camera and a fast frame grabber was used to follow the structural changes of the two samples. The samples were prepared between two Linkam glass microscopy slides with a distance of 25 μm maintained by Teflon spacers. For both compounds, a Linkam temperature control unit (THMS600), equipped with a TMS94 temperature programmer, was employed for the temperature-dependent studies. Images were recorded following slow cooling (1 K/min) from the isotropic state. Some representative POM images within the different phases are shown in Figure 1.

X-ray Scattering. Wide-angle X-ray scattering (WAXS) measurements (performed at MPI-P) were made using Cu Kα radiation from a Rigaku MicroMax 007 X-ray generator (λ = 1.54184 nm), using Osmic Confocal Max-Flux curved multilayer optics. Samples in the form of fibers were prepared with a mini-extruder at 25 and 40 °C, for C_8-BTBT and C_8-BTBT-C_8, respectively. Temperature-dependent WAXS measurements were performed by inserting the fibers into glass capillaries (1 mm diameter) at temperatures in the range from 30 to 140 °C and heating in steps of 5 °C. A waiting (equilibration) time of 1800 s and a measurement time of 1800 s was set in the temperature program. Diffraction patterns were obtained by radial averaging of the data recorded by a 2D-detector (Mar345 Image Plate).

Dielectric Spectroscopy (DS). Dielectric measurements (isothermal and isochronal) were made with a Novocontrol Alpha frequency analyzer under "isobaric" conditions. The isothermal measurements were performed at different temperatures in the range 178−423 K in steps of 5 K for C_8-BTBT and in the range 273−423 in 5 K steps and within 353−403 in steps of 2 K for C_8-BTBT-C_8 (for better observation of the SmA phase) for frequencies in the range from 10^{-2} to 10^7 Hz. The isochronal measurements were performed at f = 1154 Hz during cooling and heating at a rate of 2 K/min. The complex dielectric permittivity $\varepsilon^* = \varepsilon' - i\varepsilon''$, where ε' is the real and ε'' is the imaginary part, has been obtained as a function of frequency ω, temperature T, and dc-bias, that is, $\varepsilon^*(T, \omega)$.[19−21] The analysis of the T-dependent experiments was made using the empirical equation of Havriliak and Negami (HN):[22]

$$\varepsilon^*_{HN}(\omega, T) = \varepsilon_\infty(T) + \frac{\Delta\varepsilon(T)}{[1 + (i\omega\cdot\tau_{HN}(T))^m]^n} + \frac{\sigma_0(T)}{i\varepsilon_f\omega} \quad (1)$$

where $\varepsilon_\infty(T)$ is the high-frequency permittivity, $\tau_{HN}(T)$ is the characteristic relaxation time in this equation, $\Delta\varepsilon(T) = \varepsilon_0(T) - \varepsilon_\infty(T)$ is the relaxation strength, m, n (with limits $0 < m, mn \leq 1$) describe respectively the symmetrical and asymmetrical broadening of the distribution of relaxation times, σ_0 is the dc conductivity, and ε_f is the permittivity of free space. From τ_{HN}, the relaxation time at maximum loss, τ_{max}, is obtained analytically following

dx.doi.org/10.1021/jp412422e | J. Phys. Chem. B 2014, 118, 1443−1451

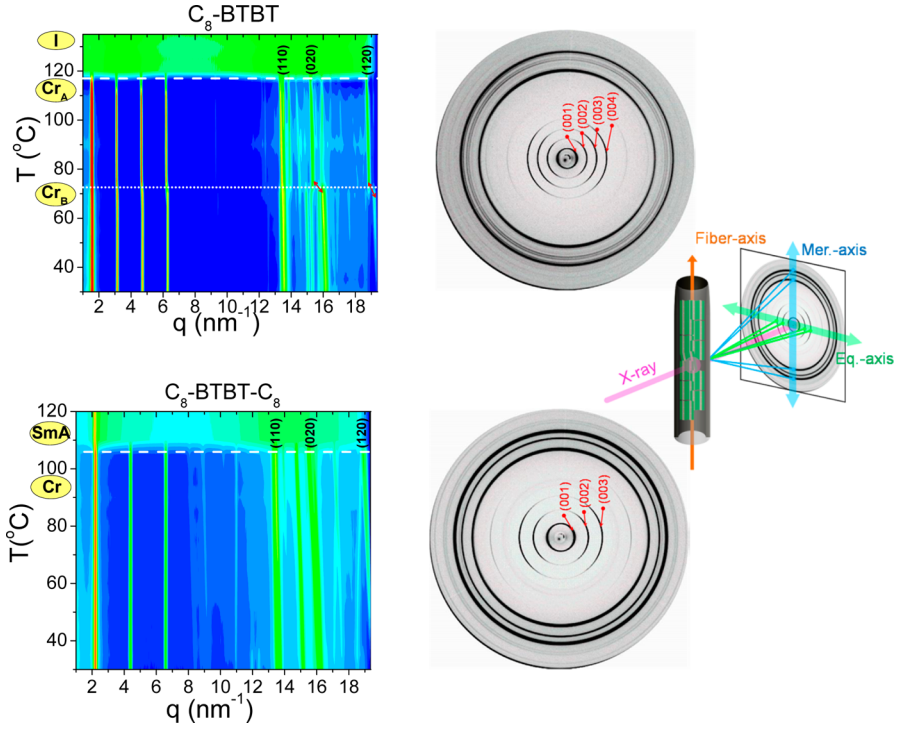

Figure 2. (Left) WAXS intensity contour plots corresponding to the phases of C_8-BTBT (top) and C_8-BTBT-C_8 (bottom). The main meridional reflections are indicated in parentheses. The horizontal dashed white lines indicate the respective transition temperatures and the white dotted line in C_8-BTBT indicate the Cr_B to Cr_A transformation. (Right) The 2D-WAXS patterns obtained from extruded fibers at 60 °C during heating, corresponding to the Cr_B phases of C_8-BTBT (top) and C_8-BTBT-C_8 (bottom). The main (00l) reflections are indicated. The X-ray and fiber geometries are also shown together with the equatorial and meridional directions.

$$\tau_{max} = \tau_{HN} \sin^{-1/m}\left(\frac{\pi m}{2(1+n)}\right)\sin^{1/m}\left(\frac{\pi mn}{2(1+n)}\right) \quad (2)$$

In addition to the measured ε'' spectra the derivative of ε' ($d\varepsilon'/d \ln \omega \sim -(2/\pi)\varepsilon''$) have been used in the analysis of the dynamic behavior. The characteristic time of ion mobility is obtained from the crossing of the real and imaginary parts of ε^* or, equivalently, of the modulus (M^*) representation ($\varepsilon^* = 1/M^*$).

Rheology. A TA Instruments rheometer (model AR-G2) with a magnetic bearing that allows for low nano torque control was used for recording the viscoelastic properties of C_8-BTBT and C_8-BTBT-C_8. Measurements were made with the environmental test chamber as a function of temperature. The samples were prepared on the lower plate of the 8, 25, 40 mm (depending on the phase of the compound) diameter parallel plate geometry and heated under nitrogen atmosphere until it could flow. Subsequently, the upper plate was brought into contact, the gap thickness was adjusted and the sample was slowly cooled to the desired starting temperature. The storage (G') and loss (G'') shear moduli were monitored in different types of experiments. First, from strain sweep experiment results the linear and nonlinear viscoelastic ranges were identified by recording the strain amplitude (γ_0) dependence of the complex shear modulus $|G^*|$ at selected temperatures (at ω = 10 rad/s). It was found that the Cr and SmA phases exhibit nonlinear response at small strain amplitudes. In subsequent experiments, strain amplitudes within the linear viscoelastic range were used as follows: γ = 0.001 within Cr phase of C_8-BTBT and γ = 0.01 and 0.00006 within the SmA and crystalline phases of C_8-BTBT-C_8. These experiments involved (i) isochronal scans at ω = 10 rad/s and (ii) isothermal scans at some selected temperatures that correspond to the Cr phase (98 and 117 °C) of C_8-BTBT-C_8 and to Cr (50 °C) and the SmA phases (88 and 100 °C) of C_8-BTBT. Finally, isochronal/isothermal time sweeps were performed to obtain the kinetics and the nature of phase transformation from the isotropic to the different ordered phases. During these experiments the strain amplitude and the size of rheometer plates were selected based on the linear properties of the newly formed phases (Cr for C_8-BTBT and SmA, Cr for C_8-BTBT-C_8). Because the viscoelastic response of structured fluids is strongly dependent on the history of deformation, all data reported here were obtained after quenching from the isotropic phase.

III. RESULTS AND DISCUSSION

Thermal and Structural Properties. The DSC thermogram for the asymmetric C_8-BTBT compound identified a strong endothermic peak associated with the crystalline (Cr) to isotropic (I) transition at 114.8 °C. In addition, a broad endothermic feature (it is actually a double peak as shown in Figure S3, Supporting Information) was found at around 55 °C associated with a structural transformation within the crystalline phase (Table 1). In the symmetric C_8-BTBT-C_8 compound, a smectic phase is formed between the crystalline and isotropic phases. The POM images identified a SmA phase.

The morphology was investigated with wide-angle X-ray scattering from extruded fibers and the results are discussed with the help of the intensity contour plots together with the 2D-patterns shown in Figure 2. The 2D-WAXS patterns reveal a set of strong equatorial reflections indexed as (00l) together with a set of meridional reflections. The latter correspond to the (110), (020), and (120) reflections from a monoclinic unit cell. From the width of the (001) reflections, the size of grains

dx.doi.org/10.1021/jp412422e | J. Phys. Chem. B 2014, 118, 1443−1451

was estimated with the Scherrer equation ($D = K\lambda/\beta \cos\theta$, where K is a constant, λ is the wavelength of X-rays, θ is the angle, and β is the full width at half-maximum intensity the latter expressed in radian) and amount to 36 and 46 nm for C_8-BTBT and C_8-BTBT-C_8, respectively. In addition, for the C_8-BTBT, a phase transition is evident at about 70 °C (different from the DSC transition probably because of the different heating rates). The crystal structure of C_8-BTBT conforms to a monoclinic unit cell with parameters a = 0.588 nm, b = 0.785, c = 4.01 nm, and β = 92.5° at temperatures below 70 °C and parameters a=0.575 nm, b = 0.825, c = 4.06 nm and β = 94° at higher temperatures. We thus refer to the low and high temperature monoclinic phases of C_8-BTBT as Cr_B and Cr_A, respectively. For the C_8-BTBT-C_8 compound, the unit cell is also monoclinic with parameters a = 0.585 nm, b = 0.789, c = 2.87 nm, and β = 91.45° in agreement with an earlier study.[6]

More informative on the structural changes within the low temperature phases of C_8-BTBT is the temperature dependence of the first equatorial (001) and main meridional reflections (110) and (020) shown in Figure 3. The figure

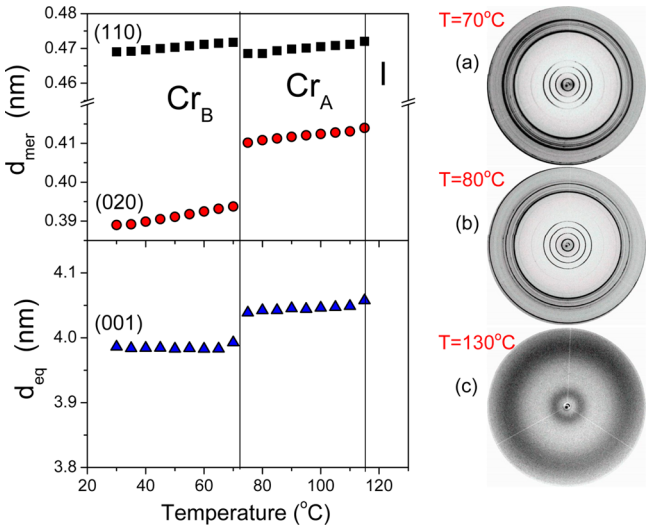

Figure 3. (Left) Temperature dependence of the main intramolecular d_{mer} (top) and intermolecular d_{eq} (bottom) distances of C_8-BTBT corresponding to the (110), (020), and (001) reflections, respectively, of the monoclinic unit cell. The vertical solid lines indicate the respective phase transition temperatures. (Right) The 2D-WAXS patterns obtained on heating at 70 °C (a), 80 °C (b), and 130 °C (c) corresponding, respectively, to the Cr_B, Cr_A, and I phases of C_8-BTBT.

depicts also 2D images at selected temperatures obtained from the same extruded fiber on heating. The phase transition at ~72 °C between the two isostructural crystalline phases is accompanied by substantial loss of orientational order.

The results of the morphology in the two compounds are shown in a highly schematic way in Figure 4. In both cases, a lamellar structure with alternating layers of BTBT and alkyl chains exist along the crystallographic c-axis. In the ab plane a herringbone arrangement of the BTBT cores has been proposed in the C_8-BTBT-C_8 case.[5,6] The figure depicts a head-to-head arrangement of C_8-BTBT molecules in a supramolecular arrangement with an interlayer distance of about 4 nm. In the C_8-BTBT-C_8 compound there is molecular order with an interlayer distance of about 2.9 nm in good agreement with earlier investigations.[6] In the asymmetric BTBT, the core layer is double in size and, as a consequence,

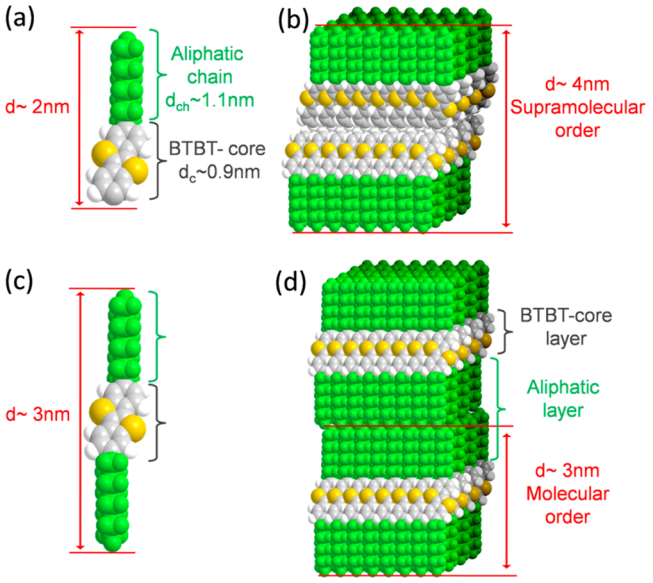

Figure 4. Highly schematic representation of the C_8-BTBT (a) and C_8-BTBT-C_8 (c) molecules together with their packing motifs within the Cr phase; (b) "head-to-head" structure of C_8-BTBT and (d) "layer-by-layer" structure of C_8-BTBT-C_8.

it has a broader network of intermolecular interactions though the increased S−S contacts. This is advantageous for the development of high performance OFET devices.

The temperature dependence of the complex dielectric constant is informative not only of the phase transformations but also of the dipolar and ionic mobility in the systems. Figure 5 compares the dielectric permittivity and loss spectra of both compounds under isochronal conditions. The static dielectric constant of polar liquids with short-range interactions between molecules has been the subject of a theory by Kirkwood and later by Fröhlich.[19,20] Fröhlich considered an infinite continuum of dielectric permittivity, ε_S', and within this a spherical region containing N_o elementary dipoles that were treated explicitly. On the basis of these assumptions, the dielectric permittivity can be expressed as

$$\varepsilon'_S = \varepsilon_\infty + \frac{1}{3\varepsilon_o} F g \frac{\mu^2}{k_B T} \frac{N_0}{V} \quad (3)$$

Here, $F = \varepsilon'_S(\varepsilon_\infty + 2)^2/[2(\varepsilon'_S + \varepsilon_\infty)]$ is the local field, N/V is the number density of dipoles expressed as $(\rho/M)N_A$, where ρ is the mass density and M is the molar mass, μ is the dipole moment, and g is the dipole orientation correlation function. Considering a reference dipole surrounded by z equivalent nearest neighbors only gives $g = 1 + z\langle\cos\theta\rangle$. Here, θ is the angle between the reference dipole and one of its z nearest neighbors. According to eq 3, ε_S' should scale with temperature as T^{-1} which is actually observed with the isotropic phases of both compounds. However, interesting effects are observed on crossing the SmA and crystalline phases. In the case of C_8-BTBT-C_8 there is a hysteresis when cooling below 0 °C with substantially larger dielectric permittivity on cooling. The hysteresis becomes very pronounced when cooling at even lower temperatures. For example, at −100 °C the dielectric permittivity drops to 2.15 from a value of 2.7 at 0 °C, in the absence of a phase transformation (DSC). A similar hysteresis is obtained for C_8-BTBT but only after cooling below −130 °C. Again the large hysteresis is not due to a phase transition but

dx.doi.org/10.1021/jp412422e | J. Phys. Chem. B 2014, 118, 1443−1451

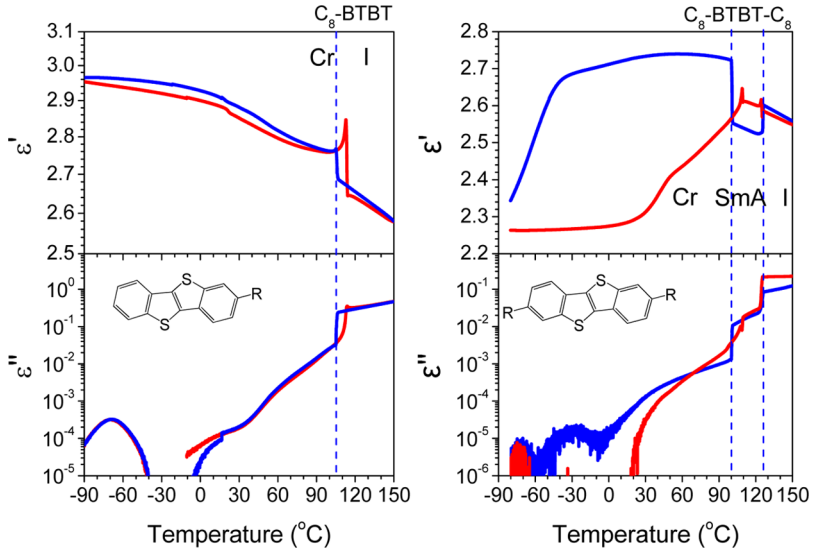

Figure 5. Temperature dependence of the dielectric permittivity, ε' (top) and loss ε'' (bottom) of C_8-BTBT (left) and C_8-BTBT-C_8 (right) obtained under isochronal conditions at f = 1154 Hz on cooling (blue) and subsequent heating (red) with 2 K/min. The vertical dashed lines indicate the respective phase transition temperatures obtained on cooling. Notice the large hysteresis in dielectric permittivity of C_8-BTBT-C_8 when cooling below 0 °C. For C_8-BTBT, a large hysteresis is also obtained when cooling below −100 °C (Figure S4, Supporting Information).

likely reflects orientation effects. The isochronal measurements of the dielectric permittivity for both compounds are shown in Figure S4, Supporting Information). This switchable permittivity in the BTBTs is of importance given the key role of the dielectric environment and molecular polarization in charge transport.[14] In addition to the hysteresis, the dielectric loss curves display some weak dielectric activity at low temperatures, that is, the peak at ∼−70 °C in C_8-BTBT (Figure 5). Notice the very weak dipolar relaxation in the symmetric compound within the Cr phase, which is expected from the absence of a dipole moment. The dielectric loss in C_8-BTBT-C_8 on entering the Cr phase is typically hundred times weaker than of the asymmetric C_8-BTBT compound.

Figure 6 gives representative dielectric loss curves of the two compounds under isothermal conditions. These representations identify not only the temperatures of phase transformation but also the dynamics within the different phases. In the case of C_8-BTBT, the isotropic to crystalline transformation is accompanied by a discontinuous reduction in the dielectric loss reflecting mainly the reduction of ion mobility. For C_8-BTBT-C_8, the two discontinuous changes correspond to the I/SmA and SmA/Cr phase transformations. Notice the weak dielectric activity within the Cr phase of C_8-BTBT-C_8, that is about 100 times weaker than in C_8-BTBT. To analyze the dielectric loss spectra of the polar C_8-BTBT compound we have employed a summation of two HN equations together with the ionic conductivity and the results on the relaxation times will be discussed later with respect to Figure 10.

Viscoelastic Properties. Processing of the compounds requires detailed knowledge of their viscoelastic properties as a function of temperature, frequency, and strain amplitude. Figure 7 gives the temperature dependence of the storage and loss moduli of both compounds under isochronal conditions on cooling and subsequent heating. All first order transitions drastically affect the shear moduli as shown by the discontinuous changes at the I−Cr and I-SmA, SmA-Cr phase transformations of C_8-BTBT and C_8-BTBT-C_8, respectively. In addition, the SmA-Cr transition exhibits a strong hysteresis. Interestingly, apart from the discontinuous

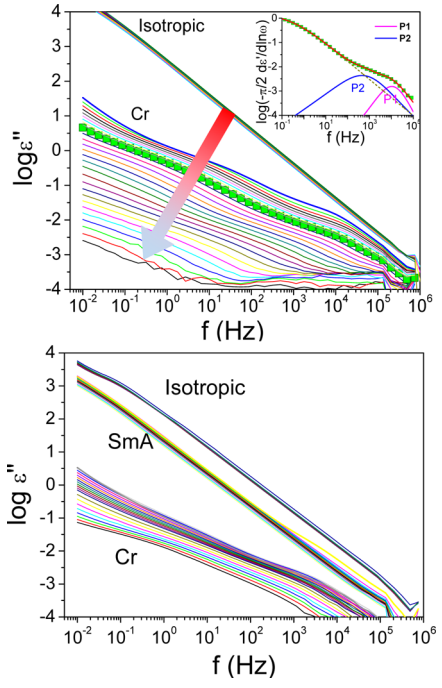

Figure 6. (Top) Typical dielectric loss (ε'') spectra of C_8-BTBT obtained on cooling from the isotropic phase indicating a strong change of ionic and dipolar dynamics. The arrow shows the direction of decreasing temperature from the isotropic (I) to the crystalline (Cr) phase. The inset gives a representable fit of the derivative of ε' at 90 °C with a sum of Havriliak−Negami functions indicated as P1 and P2. (Bottom) Corresponding dielectric loss spectra of C_8-BTBT-C_8 showing discontinuous changes at the respective transitions.

changes at the main transition temperatures the tangent delta ($\tan\delta = G''/G'$) of C_8-BTBT exhibits two weak maxima at ∼83 and 96 °C that may reflect relaxations within the Cr phase.

More information on the viscoelastic properties of the compounds can be obtained by studying the frequency response with small strain amplitudes. Unaligned smectics in particular are known to behave as "weak" viscoelastic solids

dx.doi.org/10.1021/jp412422e | J. Phys. Chem. B 2014, 118, 1443−1451

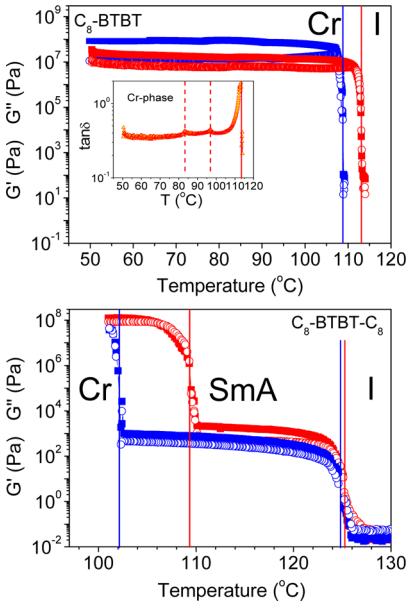

Figure 7. Temperature dependence of storage (squares) and loss (circles) moduli of C_8-BTBT (γ_0 = 0.001) (top) and C_8-BTBT-C_8 (γ_0(SmA) = 0.01; γ_0(Cr) = 0.00006) (bottom) obtained at a frequency of 10 rads^{-1} on cooling (blue) and subsequent heating (red) with 2 K min^{-1}. In the inset, the temperature dependence of the loss tangent (tanδ) of C_8-BTBT is shown. The red and blue vertical solid lines indicate the main transition temperatures on heating and cooling, respectively.

meaning that they exhibit nonlinear response at lower strain amplitudes as opposed to most viscoelastic materials.[23] In the present study, we have used as low strain amplitudes as possible within the crystal and SmA phases. In addition, in order to erase any deformation history all data were obtained by cooling from the isotropic phase. Figure 8 gives the frequency dependence of the storage and loss moduli of C_8-BTBT at three temperatures that correspond to the two monoclinic crystal phases identified by WAXS. The response within the

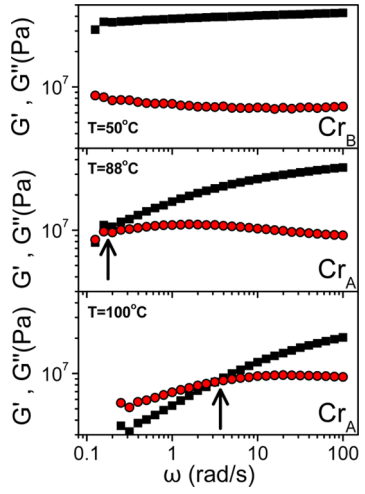

Figure 8. Frequency dependence of the storage (squares) and loss (circles) moduli of C_8-BTBT at different temperatures: 50 °C (γ_0 = 0.0001) (top), 88 °C (γ_0 = 0.0001) (middle), and 100 °C (γ_0 = 0.0001), (bottom), corresponding to Cr_B and Cr_A phases, respectively. The arrow gives the characteristic frequency, ω_X, corresponding to the crossing of the storage and loss moduli at 88 and 100 °C.

Cr_B phase at 50 °C (γ_0 = 0.0001) is elastic with $G' \sim \omega^0$ and $G'' \sim \omega^0$ at higher frequencies and an indication for a very slow relaxation at lower frequencies, suggesting suppressed mobility within the low temperature crystalline phase. However, the response within the Cr_A phase is distinctly different. At 88 °C (γ_0 = 0.0001) and 100 °C (γ_0 = 0.0001), the response is viscoelastic and a characteristic frequency can be obtained from the crossing of the storage and loss moduli at 0.178 and 3.6 rad/s, respectively. A characteristic length of defect structure[23] can be estimated from the (high) value of the storage modulus at the crossing as $G' = k_BT/d^3(\omega_c\tau)^2$, resulting to 0.8 and 0.9 nm, respectively, at 88 and 100 °C. This value suggests localized defects within the Cr_A phase. The behavior of C_8-BTBT-C_8 is different (Figure 9). The response at 98 °C (γ_0 =

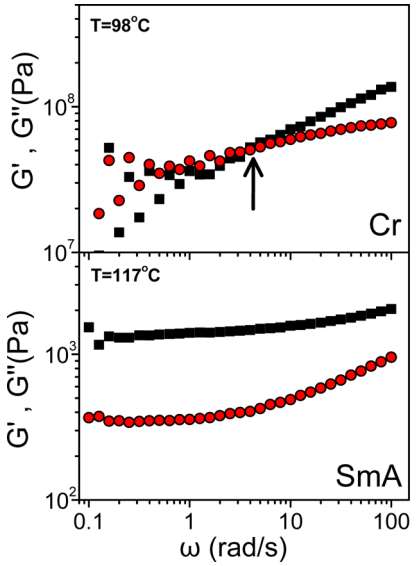

Figure 9. Frequency dependence of the storage (squares) and loss (circles) moduli of C_8-BTBT-C_8 at 98 °C (γ_0 = 0.00006) (top) and 117 °C (γ_0 = 0.01) (bottom), corresponding to the crystalline and SmA phases, respectively. The arrow gives the characteristic frequency, ω_X, at the crossing of the storage and loss moduli at 98 °C.

0.00006), that is, within the crystalline phase, is viscoelastic with a characteristic length scale of defect structure of only 0.5 nm. However, the response at 117 °C (γ_0 = 0.01), corresponding to the SmA phase, is that of a viscoelastic solid with a modulus of $G = 1.4 \times 10^3$ Pa.

Dynamics. The dynamics of rodlike liquid crystals have been studied extensively with DS mainly within the nematic phase. The dynamics reflect rotations about their long and short molecular axes.[24−26] This gives rise to a "fast" (called α) and to a hindered, that is, "slow" process (called δ) that are very distinct within the nematic phase because the nematic potential hinters the rotation about the short axis. The intensity of the two modes depends on the orientation of the director with respect to the external electric field. For example, a director aligned parallel (perpendicular) to the electric field favors relaxation through the slower (faster) process. The asymmetric compound C_8-BTBT possess a weak dipole moment (μ = 0.99 D using MOPAC2007, PM6) along the long molecular axis that allows probing the molecular dynamics. However, within the isotropic phase the molecular dynamics are faster than the experimentally accessible window (Figure 6) and only the ion mobility contributes to the measured frequency range. Ion

dx.doi.org/10.1021/jp412422e | J. Phys. Chem. B 2014, 118, 1443−1451

mobility is distinctly different within the different phases and can be used as a fingerprint to the phase transitions. This is depicted in Figure 10, where the ion mobility obtained from the

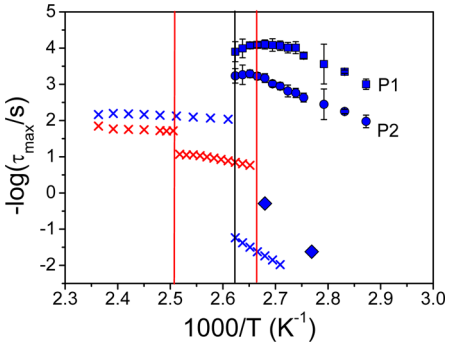

Figure 10. Arrhenius relaxation map of C_8-BTBT: the two closely spaced processes (P1 and P2) within the Cr-phase and the process of ionic mobility (x) are shown. Vertical solid lines indicate the transition temperatures of C_8-BTBT (blue) and of C_8-BTBT-C_8 (red) obtained from discontinuous changes in the ionic conductivity. The ultraslow process (rhombi) of C_8-BTBT from rheology is also shown, for comparison.

crossing of the real and imaginary parts of ε^* (or M^*) are plotted in an Arrhenius representation for C_8-BTBT (in blue) and C_8-BTBT-C_8 (in red). There is a discontinuous decrease of ion mobility at the SmA and Cr phases.

With respect to the molecular processes of C_8-BTBT within the Cr_A phase, two closely spaced in frequency processes contribute to the dielectric loss described as P1 and P2. These processes likely reflect remnants of the δ-process but with suppressed intensity because of the stronger potential within the crystalline phase. Rheology identifies in addition a slower relaxation of viscoelastic nature within the Cr_A phase. The process reflects the defect structure within the Cr_A phase. These results reveal that there is some molecular mobility within the high temperature crystalline phase of C_8-BTBT with the viscoelastic character.

Kinetics of Structure Formation. The viscoelastic contrast between the I, SmA, and Cr phases of the BTBT compounds allow an investigation of the kinetics of phase transformation from the initial isotropic phase to the different ordered phases. In these experiments, the evolution of the storage and loss shear moduli is probed following a temperature jump from the same initial temperature (135 °C for the I/SmA and 120 °C for the SmA/Cr transformations in C_8-BTBT-C_8 and 130 °C C_8-BTBT, respectively) to different final temperatures corresponding to the SmA and Cr phases of C_8-BTBT-C_8 and to the Cr_A phase of C_8-BTBT (Figure 11). We first examine the kinetics of the I-to-SmA transformation in C_8-BTBT-C_8. The modulus displays a sigmoidal shape during the transformation from the initial undercooled isotropic phase (shown with the line in Figure 11) to the final SmA phase. Alternatively, the kinetics of the SmA to Cr phase display a drastic increase from the initial undercooled SmA phase (solid line in Figure 11 at $|G^*| \sim 10^3$ Pa) to the final crystalline phase. In all cases, increasing the final temperature shifts the curves to longer times which suggests that the kinetics are controlled by nucleation barriers, that is, typical of the nucleation and growth type. To obtain the time-scale and the details of transformation a two-phase system is assumed comprising two phases whose relative contribution evolve with time.[27] The rheological response of such "composites" can be very complex;[28] herein we employ the simplest "parallel" and "series" models that provide an upper and a lower bound for the modulus. The upper bound refers to the limiting case of a homogeneous distribution of strain. The modulus of the two phase system can be expressed as a linear combination of the moduli of the constituent phases as

$$G^* = \varphi_{Cr} G^*_{Cr} + \varphi_{Lc} G^*_{Lc} \quad (4)$$

where φ is the volume fraction and A, B refer to the moduli of the final and initial phases, respectively. The lower bound refers

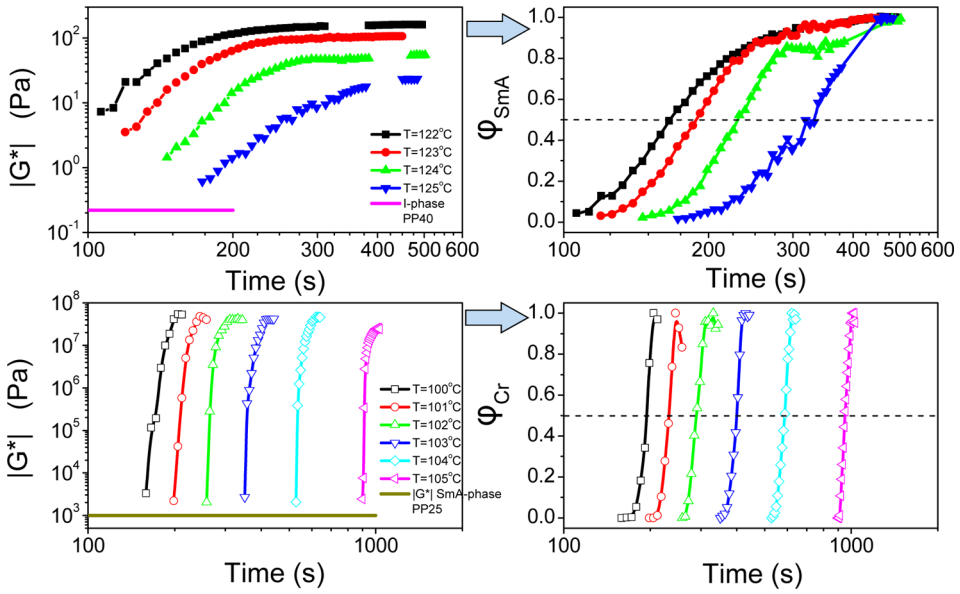

Figure 11. (Left) Evolution of the complex shear modulus during the transformations I/SmA (γ_0 = 0.01) (top) and SmA/Cr (γ_0 = 0.00006) (bottom) of C_8-BTBT-C_8. (Right) Extracted volume fractions of the SmA and Cr phases during the respective transformations. The horizontal solid lines indicate a volume fraction of 0.5.

dx.doi.org/10.1021/jp412422e | J. Phys. Chem. B 2014, 118, 1443−1451

to the limiting case of a homogeneous distribution of the stress. In this case, the compliance of the two phase system can be expressed as a linear combination of the compliances of the constituent phases as

$$J^* = \varphi_{Cr} J^*_{Cr} + \varphi_{Lc} J^*_{Lc} \quad (5)$$

The time dependence of the volume fraction of the SmA and C_r phases of C_8-BTBT-C_8 as obtained through the parallel model is also shown in Figure 11.

There are several examples in soft matter physics (ordering in block copolymers,[29,30] polymer crystallization,[31] structure formation in discotic liquid crystals[32,33]) where structure formation proceeds via a nucleation and growth mechanism. For a nucleation and growth process, the time-dependence of the volume fractions of the newly formed phases is usually described by the Avrami equation[34]

$$\varphi_{Cr} = 1 - \exp(-zt^n) \quad (6)$$

In the above equation, z gives the rate of nucleation and growth and the exponent n has contributions from the time-dependence of the nucleation and growth process (i.e., athermal vs thermal) and the dimensionality of growth. From z, the half-time of crystallization can be obtained as $t_{1/2} = (\ln 2/z)^{1/n}$. Here because of the sharp increase of φ_{Cr} we chose to obtain the characteristic transformation time corresponding to $\varphi = 0.5$ (dashed line in Figure 11).

The thus obtained characteristic times are shown in Figure 12 as a function of the quench depth, $\Delta T = T_f - T_i$. In all transformations, much longer characteristic times are obtained for the shallower quenches. In C_8-BTBT-C_8, the formation of the SmA from the isotropic phase proceeds much faster than the crystalline phase from the SmA phase under identical quench depth. As for the I to Cr transformation in C_8-BTBT, it appears to have the same activation barrier as the SmA to Cr transformation in C_8-BTBT-C_8. In any case, there results suggest nucleation and growth mechanism with rather low activation barriers that should be considered when crossing boundaries between the different ordered phases.

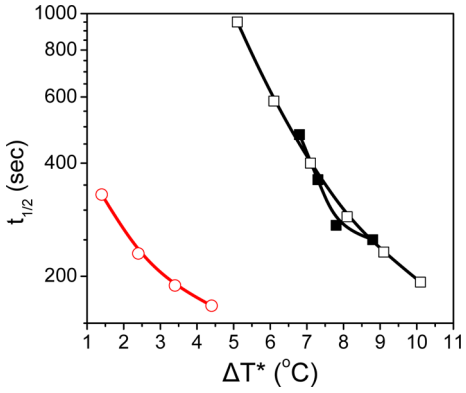

Figure 12. Characteristic half-times of the phase transformations plotted as a function of reduced temperature, ΔT^*, obtained from rheology corresponding to the I/Cr transformation of C_8-BTBT (filled squares) and to the I/SmA (open circles) and SmA/Cr (open squares) transformations of C_8-BTBT-C_8.

IV. CONCLUSION

The main results from the thermodynamic, structural, and dynamic investigations by X-rays, rheology, and dielectric spectroscopy experiments in symmetrically and asymmetrically substituted BTBTs can be summarized as follows:

- In both the symmetric and the asymmetric BTBTs, a lamellar structure with alternating layers of BTBT and alkyl chains exist along the crystallographic c-axis. However, in C_8-BTBT a head-to-head arrangement of molecules in a supramolecular arrangement is found with an interlayer distance of about 4 nm. This contrasts with the molecular order in C_8-BTBT-C_8 with an interlayer distance of 2.9 nm. The existence of a broader 2D semiconducting layer with a network of intermolecular interactions in the asymmetric BTBT compound is advantageous for the development of high-performance OFET devices.
- A smectic phase is absent in the asymmetric C_8-BTBT. Two isostructural crystal phases were identified by X-rays with slightly different parameters of their monoclinic unit cells. The low-temperature crystalline phase is purely elastic and the high temperature phase is viscoelastic. On the other hand, the SmA phase in C_8-BTBT-C_8 can be described as viscoelastic solid of low modulus.
- A path-dependent dielectric environment with a switchable dielectric permittivity was found in both compounds by cooling below 0 °C. This effect is very pronounced in the symmetric compound. On the other hand, the asymmetric BTBT compound is more advantageous as the dielectric permittivity exhibits only minor hysteresis down to 0 °C.
- This effect needs to be explored further in view of the key role of dielectric environment to charge transport.
- Within the high-temperature crystalline phase of C_8-BTBT there is substantial molecular mobility over a broad frequency range (0.1 to 10^6 Hz) associated with restricted molecular dynamics (DS) and defect motion (rheology).
- The kinetics of phase transformation to the crystalline and SmA phases revealed typical nucleation and growth processes where the rates are dominated by low activation barriers.

These results show that the morphology, dielectric, and viscoelastic properties of BTBTs depend largely on processing conditions. For example, cooling below 0 °C drastically changes the dielectric permittivity of the symmetric compound. To the extent that the intrinsic dielectric response of the material is determining the charge carrier mobility this is of paramount importance to device performance. Future research efforts should be directed toward associating the reported charge carrier mobilities to these characteristics aiming at optimizing performance.

■ ASSOCIATED CONTENT

Supporting Information

Synthesis and potential impurities, ^{1}H NMR spectra as well as isochronal DS measurements showing switchable permittivity in the C_8-BTBT and C_8-BTBT-C_8 compounds. This material is available free of charge via the Internet at http://pubs.acs.org.

■ AUTHOR INFORMATION

Notes

The authors declare no competing financial interest.

■ ACKNOWLEDGMENTS

G.F. acknowledges support by the MPI-P during his sabbatical leave. The current work was supported by the Research unit on Dynamics and Thermodynamics of the UoI cofinanced by the European Union and the Greek state under NSRF 2007-2013 (Region of Epirus, call 18). This work was cofinanced by the

E.U.- European Social Fund and the Greek Ministry of Development - GSRT in the framework of the programs HERAKLEITOS and THALIS. This work has also been financially supported by a concerted research action of the French Community of Belgian (ARC project no. 20061), and by the Walloon Region (WCS project no. 1117306).

REFERENCES

(1) Mei, J.; Diao, Y.; Appleton, A. L.; Fang, L.; Bao, Z. Integrated Materials Design of Organic Semiconductors for Field-Effect Transistors. *J. Am. Chem. Soc.* **2013**, *135*, 6724−6746.
(2) Minemawari, H.; Yamada, T.; Matsui, H.; Tsutsumi, J.; Haas, S.; Chiba, R.; Kumai, R.; Hasegawa, T. Inkjet printing of single-crystal films. *Nature* **2011**, *475*, 364−367.
(3) Diao, Y.; Tee, B.C.-K.; Giri, G.; Xu, J.; Kim, D. H.; Becerril, H. A.; Stoltenberg, R. M.; Lee, T. H.; Xue, G.; Mannsfeld, S. C. B.; Bao, Z. Solution coating of large-area organic semiconductor thin films with aligned single-crystalline domains. *Nat. Mater.* **2013**, *12*, 665−671.
(4) Giri, G.; Verploegen, E.; Mannsfeld, S. C. B.; Atahan-Eurenk, S.; Kim, D. H.; Lee, S. Y.; Becerril, H. A.; Apsuru-Guzik, A.; Toney, M. F.; Bao, Z. Tuning charge transport in solution-sheared organic semiconductors using lattice strain. *Nature* **2011**, *480*, 504−508.
(5) Ebata, H.; Izawa, T.; Miyazaki, E.; Takimiya, K.; Ikeda, M.; Kuwabara, H.; Yui, T. Highly Soluble [1]Benzothieno[3,2-b]-benzothiophene (BTBT) Derivatives for High-Performance, Solution-Processed Organic Field-Effect Transistors. *J. Am. Chem. Soc.* **2007**, *129*, 15732−15733.
(6) Izawa, T.; Miyazaki, E.; Takimiya, K. Molecular Ordering of High-Performance Soluble Molecular Semiconductors and Re-evaluation of Their Field-Effect Transistor Characteristics. *Adv. Mater.* **2008**, *20*, 3388−3392.
(7) Amin, A. Y.; Reuter, K.; Meyer-Friedrichsen, T.; Halik, M. Interface Engineering in High-Performance Low-Voltage Organic Thin-Film Transistors Based on 2,7-Dialkyl-[1]benzothieno[3,2-b][1]benzothiophenes. *Langmuir* **2011**, *27*, 15340−15344.
(8) Amin, A. Y.; Khassanov, A.; Reuter, K.; Meyer-Friedrichsen, T.; Halik, M. Low-Voltage Organic Field Effect Transistors with a 2-Tridecyl[1] benzothieno[3,2-b][1]benzothiophene Semiconductor Layer. *J. Am. Chem. Soc.* **2012**, *134*, 16548−16550.
(9) Ruzié, C.; Karpinska, J.; Kennedy, A. R.; Geerts, Y. H. Synthesis of 1,6-, 2,7-, 3,8-, and 4,9-Isomers of Didodecyl[1]benzothieno[3,2-b][1]benzothiophenes. *J. Org. Chem.* **2013**, *78*, 7741−7748.
(10) Lino, H.; Kobori, T.; Hanna, J.-I. High Uniformity and High Thermal Stability of Solution-Processed Polycrystalline Thin Films by Utilizing Highly Ordered Smectic Liquid CrystalsJpn. *J. Appl. Phys.* **2012**, *51*, 11PD02.
(11) Vehoff, T.; Chung, Y. S.; Johnston, K.; Troisi, A.; Yoon, D. Y.; Andrienko, D. Charge Transport in Self-Assembled Semiconducting Organic Layers: Role of Dynamic and Static Disorder. *J. Phys. Chem. C* **2010**, *114*, 10592−10597.
(12) Hansen, M. R.; Feng, X.; Macho, V.; Müllen, K.; Spiess, H. W.; Floudas, G. Fast and Slow Dynamics in a Discotic Liquid Crystal with Regions of Columnar Order and Disorder. *Phys. Rev. Lett.* **2011**, *107*, 257801−257805.
(13) Duran, H.; Hartmann-Azanza, B.; Steinhart, M.; Gehrig, D.; Laquai, F.; Feng, X.; Müllen, K.; Butt, H.-J.; Floudas, G. Arrays of Aligned Supramolecular Wires by Macroscopic Orientation of Columnar Discotic Mesophases. *ACS Nano* **2012**, *6*, 9359−9365.
(14) Minder, N. A.; Ono, S.; Chen, Z.; Facchetti, A.; Morpurgo, A. F. Band-Like Electron Transport in Organic Transistors and Implication of the Molecular Structure for Performance Optimization. *Adv. Mater.* **2012**, *24*, 503−508.
(15) Xie, W.; Willa, K.; Wu, Y.; Häusermann, R.; Tukimiya, K.; Batlogg, B.; Frisbie, C. D. emperature-Independent Transport in High-Mobility Dinaphtho-Thieno-Thiophene (DNTT) Single Crystal Transistors. *Adv. Mater.* **2013**, *25*, 3478−3484.
(16) Saito, M.; Osaka, I.; Miyazaki, E.; Takimiya, K.; Kuwabara, H.; Ikeda, M. One-step synthesis of [1]benzothieno[3,2-b][1]-benzothiophene from o-chlorobenzaldehyde. *Tetrahedron Lett.* **2011**, *52*, 285−288.
(17) Košata, B.; Kozmik, V. Svoboda, Reactivity of [1]benzothieno-[3,2-b][1]benzothiophene - Electrophilic and metallation reactions. *J. Collect. Czech. Chem. Commun.* **2002**, *67*, 645−664.
(18) Košata, B.; Kozmik, V.; Svoboda, J.; Novotná, V.; Vaněk, P.; Glogarová, M. Novel liquid crystals based on [1]benzothieno[3,2-b][1]benzothiophene. *Liq. Cryst.* **2003**, *30*, 603−610.
(19) Kremer, F.; Schönhals, A. In *Broadband Dielectric Spectroscopy*; Springer: Berlin, 2002.
(20) McCrum, N. G.; Read, B. E.; Williams, G. In *Anelastic and Dielectric Effects in Polymeric Solids*; Dover Publ. In.: New York, 1991.
(21) Floudas, G. In *Dielectric Spectroscopy*. Matyjaszewski, K., Möller, M., Eds.; Polymer Science: A Comprehensive Reference; Elsevier BV: Amsterdam, 2012; Vol. 2.32, pp 825−845.
(22) Havriliak, S.; Negami, S. A complex plane representation of dielectric and mechanical relaxation processes in some polymers. *Polymer* **1967**, *8*, 161−210.
(23) Colby, R. H.; Ober, C. K.; Gillmor, J. R.; Connelly, R. W.; Duong, T.; Galli, G.; Laus, M. Smectic rheology. *Rheol. Acta* **1997**, *36*, 498−504.
(24) Attard, G. S.; Araki, K.; Moura-Ramos, J. J.; Williams, G. Molecular dynamics and macroscopic alignment properties of thermotropic liquid-crystalline side chain polymers as studied by dielectric relaxation spectroscopy. *Liq Cryst.* **1988**, *3*, 861−879.
(25) Bras, A. R.; Dionisio, M.; Huth, H.; Schick, Cr.; Schönhals, A. Origin of glassy dynamics in a liquid crystal studied by broadband dielectric and specific heat spectroscopy. *Phys. Rev. E.* **2007**, *75*, 061708.
(26) Grigoriadis, C.; Duran, H.; Steinhart, M.; Kappl, M.; Butt, H.-J.; Floudas, G. Suppression of Phase Transitions in a Confined Rodlike Liquid Crystal. *ACS Nano* **2011**, *5*, 9208−9215.
(27) Ferry, J. D. *Viscoelastic Properties of Polymers*, 3nd ed.; Wiley: New York, 1980.
(28) Alig, I.; Tadjbakhsch, S.; Floudas, G.; Tsitsilianis, C. Viscoelastic Contrast and Kinetic Frustration during Poly(ethylene oxide) Crystallization in a Homopolymer and a Triblock Copolymer. Comparison of Ultrasonic and Low-Frequency Rheology. *Macromolecules* **1998**, *31*, 6917−6925.
(29) Floudas, G.; Pakula, T.; Fischer, E. W.; Hadjichristidis, N.; Pispas, S. Ordering kinetics in a symmetric diblock copolymer. *Acta Polym.* **1994**, *45*, 176−181.
(30) Floudas, G.; Ulrich, R.; Wiesner, U.; Chu, B. Nucleation and growth in order-to-order transitions of a block copolymer. *Europhys. Lett.* **2000**, *50*, 182−188.
(31) Mierzwa, M.; Floudas, G. Real-time crystallization and melting of poly(n-octadecyl methacrylate) induced by temperature and pressure - A dielectric spectroscopy investigation. *IEEE Trans. Dielectr. Electr. Insul.* **2001**, *8*, 359−364.
(32) Grigoriadis, C.; Haase, N.; Butt, H.-J.; Müllen, K.; Floudas, G. To tilt or not to tilt? Kinetics of structure formation in a discotic liquid crystal. *Soft Matter* **2011**, *7*, 4680−4689.
(33) Tasios, N.; Grigoriadis, C.; Hansen, H. R.; Wonneberger, H.; Li, C.; Spiess, H. W.; Müllen, K.; Floudas, G. Self-Assembly, Dynamics, and Phase Transformation Kinetics of Donor−Acceptor Substituted Perylene Derivatives. *J. Am. Chem. Soc.* **2010**, *132*, 7478−7487.
(34) (a) Avrami, M. Kinetics of phase change. I: General theory. *J. Chem. Phys.* **1939**, *7*, 1103−1112;(b) Kinetics of phase change. II Transformation-time relations for random distribution of nuclei. *J. Chem. Phys.* **1940**, *8*, 212−224;(c) Granulation, phase change, and microstructure kinetics of phase change. III. *J. Chem. Phys.* **1941**, *9*, 177−184.